Available online at www.sciencedirect.com

ScienceDirect

Ceramics International 40 (2014) 1851–1858

CERAMICS INTERNATIONAL

www.elsevier.com/locate/ceramint

Mo-doped indium oxide films by dip-coating: Synthesis, microstructure and optical properties

Francesca Nanni[a], Francesca Romana Lamastra[b], Fabio Franceschetti[a], Francesco Biccari[c], Ilaria Cacciotti[a,*]

[a]University of Rome "Tor Vergata", Department of Industrial Engineering, INSTM RU Tor Vergata, Via del Politecnico 1, 00133 Rome, Italy
[b]Italian Interuniversity Consortium on Materials Science and Technology (INSTM), Research Unit Roma Tor Vergata, Via del Politecnico 1, 00133 Rome, Italy
[c]ENEA, Casaccia Research Center, Via Anguillarese 301, 00123 Rome, Italy

Received 20 June 2013; accepted 17 July 2013
Available online 7 August 2013

Abstract

Molybdenum doped indium oxide ($In_{2-x}Mo_xO_3$, IMO) is widely used in many electronic and optoelectronic devices due to its excellent electrical properties and optical transparency. In this work, a first attempt to produce IMO films by sol–gel dip coating was reported, starting from different reagents (i.e. indium nitrate or indium chloride and molybdenum chloride or ammonium molybdate as In and Mo sources, respectively). The influence of different reagents, solvents and annealing atmospheres (i.e. air and N_2) on final coating properties was investigated in order to properly select the optimal process parameters. The morphological, microstructural and optical properties of the produced coatings were evaluated by scanning electron microscopy (SEM), X-ray diffractometry (XRD) and UV–vis spectroscopy. The best performances, in terms of microstructure and transparency, were obtained for films produced by dip coating the indium nitrate and molybdenum chloride based solutions (In nitrate concentration 0.1–0.2 M), with the addition of a low amount of PEG, followed by annealing at 500 °C. The produced coatings consisted of monophasic In_2O_3 and were characterised by a uniform, homogeneous and cracks free surface, and high transmittance values in the vis range (i.e. 85–98%).

Keywords: A. Films; A. Sol–gel processes; B. Microstructure; C. Optical properties; D. Molybdenum doped indium oxide (IMO)

1. Introduction

The market related to the fabrication of transparent conducting oxide (TCO) materials is in rising and ongoing expansion. Thus further and deep research about innovative and promising TCOs is strongly motivated, due to their outstanding potential applications as transparent electrodes for flat panel displays, transparent electrodes for photovoltaic cells, low emissivity windows, window defrosters, transparent thin films transistors, light emitting diodes, and semiconductor lasers.

The most widely studied TCO semiconductors are impurity-doped ZnO, In_2O_3, SnO_2 and CdO, as well as the ternary compounds Zn_2SnO_4, $ZnSnO_3$, $Zn_2In_2O_5$, $Zn_3In_2O_6$, In_2SnO_4, $CdSnO_3$, and multi-component oxides consisting of combinations of ZnO, In_2O_3 and SnO_2 [1]. The coexistence of electrical conductivity and optical transparency in these materials depends on the nature, number, and atomic arrangements of metal cations in crystalline or amorphous oxide structures, on the morphology, and on the presence of defects. The achievement of the simultaneous combination of optimal conductivity and transparency is usually impossible in intrinsic stoichiometric oxides, and requires the introduction of properly selected dopants within the oxides lattice, in order to achieve improved electrical conductivity without degrading their optical transmission [1].

In the case of In_2O_3, several dopant ions, such as tin (Sn), gallium (Ga), copper (Cu), zirconium (Zr), erbium (Er), titanium (Ti) and molybdenum (Mo) have been considered and extensively exploited [2–7]. Among them, up to now, tin doped indium oxide (ITO) is dominating the market. Recently a lot of attention has been devoted to the production of Mo doped In_2O_3 (IMO) [8], since, compared to ITO, it presents a remarkably decreased resistivity, higher spectral transmittance due to a

*Corresponding author. Tel.: +39 0672594482; fax: +39 0672594328.
E-mail address: ilaria.cacciotti@uniroma2.it (I. Cacciotti).

0272-8842/$ - see front matter © 2013 Elsevier Ltd and Techna Group S.r.l. All rights reserved.
http://dx.doi.org/10.1016/j.ceramint.2013.07.087

valance difference of three between the dopant ion (Mo^{6+}) and the substituted one (i.e. In^{3+}) [9], and a mobility more than twice that of ITO [10].

However, in the selection of the TCO materials the economical factor cannot be neglected, depending on both the used raw materials and the employed deposition technique.

Despite indium is an expensive metal, at present the performance of In free TCOs is still far from being a real commercial alternative. Therefore more attention should be devoted to find proper alternatives to the commonly used high quality and high cost vacuum deposition techniques, such as evaporation, sputtering, spray pyrolysis, atomic layer deposition (ALD), ion-assisted deposition (IAD), pulsed laser deposition (PLD), chemical vapour deposition (CVD) and plasma-enhanced chemical vapour deposition (PECVD) [11].

Many efforts are currently dedicated to the set-up of low cost large area deposition techniques, starting from cheap raw reagents and solvents, i.e. solution-based processes [12–20], such as spin-coating, dip-coating, printing (ink-jet, microcontact, etc.), and chemical bath deposition (CBD).

In particular, sol–gel based synthesis strategies appear an attractive option [21,22], featuring inherent simplicity, reliability, versatility and reproducibility of both solution phase chemistry and deposition processes, as well as an easy industrial upscaling toward large area applications. The employment of this process provides many advantages: (i) the process does not require high-maintenance and expensive vacuum pumps and chambers which are associated with vapour deposition; (ii) it is based on green chemistry and does not pose any significant process hazard or environmental concern; (iii) the doping level, solution concentration, and homogeneity are easily controlled without using expensive and complicated equipment; and (iv) this kind of method allows industrial scalability and the simultaneous preparation of a high number of films, thus increasing the production rate [23].

Even if standard sol–gel processes for TCO materials commonly use metal alkoxide precursors, the use of nonalkoxide precursors would be desirable, due to the unavailability and high cost of some metal alkoxides and the remarkable dissimilar hydrolysis rates of different metal alkoxides, therefore avoiding the preparation of mixed oxide materials [24–29].

On the ground of all these considerations and previous results, in this work a first attempt to produce IMO coatings by dip-coating process starting from sol–gel precursor solutions is reported. To the best of authors' knowledge, up to date, the fabrication of IMO films by dip-coating has not been reported yet.

The main objective was to properly set up the experimental procedure, in order to accomplish a strict control of the products in terms of chemical composition, morphology, microstructure and optical properties, by the systematic modulation of the synthesis process parameters (reagent kinds and concentrations, solvents, polymer addition) and of the thermal post-deposition treatment.

Aimed at achieving this ambitious purpose, the morphology of the obtained coatings was investigated by scanning electron microscopy (SEM), the microstructure by X-ray diffraction (XRD) analysis and the optical characteristics by UV–vis spectroscopy.

2. Materials and methods

2.1. Sol–gel indium molybdenum oxide solutions

Three IMO precursor solutions were prepared by sol–gel process, starting from different reagents as In and Mo sources, respectively.

Route I: indium nitrate hydrate ($In(NO_3)_3 \cdot H_2O$, Sigma-Aldrich, 99.90%) and ammonium molybdate tetrahydrate ($(NH_4)_8Mo_7O_{24} \cdot 4H_2O$, Sigma-Aldrich, 99.98%).
Route II: indium trichloride ($InCl_3$, Sigma-Aldrich, 99.99%) and molybdenum pentachloride ($MoCl_5$, Sigma-Aldrich, 99.99%).
Route III: indium nitrate hydrate ($In(NO_3)_3 \cdot H_2O$, Sigma-Aldrich, 99.90%) and molybdenum pentachloride ($MoCl_5$, Sigma-Aldrich, 99.99%).

In a first preliminary phase, the process parameters were set up and properly monitored, in terms of reagent kinds and concentrations, solvents and mixtures of solvents, addition of

Table 1
Sample nomenclature of IMO films and major properties of starting solutions (stoichiometric Mo content 1 at%).

Sample	Route	Precursor	[In source] (M)	Solvent	Polymer	Number of dipping
N1	I	$In(NO_3)_3 \cdot H_2O$ $(NH_4)_8Mo_7O_{24} \cdot 4H_2O$	1.5	dH_2O	–	3
N1_PVA			1.5	dH_2O	PVA	3
N2			1.5	dH_2O:EtOH, 1:1	–	6
C1	II	$InCl_3$+$MoCl_5$	1.5	dH_2O	–	3
C1_PVA			1.0	dH_2O	PVA	6
C2			2.0	MeOH:GAA, 1:1	–	3
C2_PEG			2.0	MeOH:GAA, 1:1	PEG	3
C3			0.2	EtOH:GAA, 1:1	–	8
C3_PEG			0.2	EtOH:GAA, 1:1	PEG	8
NC1_PVA	III	$In(NO_3)_3 \cdot H_2O$+$MoCl_5$	1.5	dH_2O	PVA	6
NC2_PEG			0.1	EtOH:GAA, 1:1	PEG	8
NC3			0.2	EtOH:GAA, 1:1	–	6
NC3_PEG			0.2	EtOH:GAA, 1:1	PEG	8

polymer as a template (Table 1). In details the indium source reagent concentration ranged between 0.1 M and 2 M, in order to identify the most appropriate one, whereas, in all cases, on the basis of the literature data [30,31], a Mo dopant amount of 1 at% was selected.

The solutions were prepared both with and without the addition of a polymer (1 wt%/v), i.e. polyvinylalcohol (PVA, $(C_2H_4O)_x$, Mw 130,000, Sigma-Aldrich) and polyethylene glycol (PEG, $C_{2x}H_{4x+2}O_{x+1}$, intrinsic density 1.13 g/cm^3, Fluka-Sigma-Aldrich). Specifically, for the preparation of PVA solution, the polymer was dissolved in the solvent at 80 °C for 2 h under continuous magnetic stirring and then left to cool at room temperature for further 2 h.

As a reference, undoped In_2O_3 precursor solution was also prepared using an indium nitrate hydrate concentration of 0.1 M.

2.2. Dip-coating

IMO films were deposited on microscopic soda-lime glass slides (Menzel Gläser) by the dip-coating procedure, starting from sol–gel derived solutions. All depositions were carried out at room temperature, up to a maximum of eight times. Prior to the coating process, glass slide substrates (26 mm × 76 mm × 1 mm) were rinsed in acetone using a standard ultrasonic cleaner and subsequently dried in air.

The glass substrates were dipped in the solutions of In- and Mo-based precursors and withdrawn at a rate of 4 cm/min. The deposited layers were then dried at room temperature for 30 min and afterwards submitted to a properly programmed thermal cycle after each dipping. The thermal annealing (selected on the basis of thermal analysis results, see later on) was carried out in air and consisted of three steps: a first one up to 90 °C for 2 h (heating rate 2 °C/min), a second one up to 500 °C for 2 h (heating rate 2 °C/min), and finally the last one up to room temperature (cooling rate 2 °C/min).

The above cycle (dipping–drying–heating) was repeated several times (up to eight times) giving rise to multilayer IMO films.

In Table 1 nomenclatures and solution characteristics of all produced samples are collected.

Finally, in selected cases, the same thermal treatment cycle was performed in controlled inert N_2 atmosphere.

2.3. Characterisation

The thermal behaviour of the prepared solutions was investigated by simultaneous thermogravimetry and differential thermal analysis (TG–DTA, Netzsch STA 409; sample weight ~90 mg, heating rate 10 °C/min, peak temperature 1100 °C, air flow 80 cc/min).

Phase analysis of all samples was performed by means of X-ray diffraction (Philips X'Pert 1710, Cu Kα radiation $\lambda = 1.5405600$ Å, $2\theta = 10$–$80°$, step size = 0.020°, time per step = 2 s, scan speed = 0.01 deg/s).

XRD measurements were also used to investigate preferred grain orientation and to evaluate the average crystallite size (τ). The τ values of all samples were obtained by means of Debey–Scherrer's equation

$$\tau_{(hkl)} = \frac{K\lambda}{\sqrt{\varpi^2 - \varpi_0^2}\cos\vartheta} \quad (1)$$

where K is the shape factor equal to 0.9, λ is the X-ray wavelength (i.e. 1.541 Å for Cu Kα radiation), θ is the Bragg angle, ω is the full width at half maximum (FWHM) and, ω_0 is the instrumental width (i.e. 0.087). The τ values were determined using the half width of the diffraction peak at $2\theta = 30.5°$ corresponding to the (222) Miller plane family of In_2O_3 (JCPDS # 76-0152).

In selected cases, the cell parameters were estimated through the algorithm TREOR (Philips X'Pert Plus software), considering the JCPDS Card no. 76-0152 for the In_2O_3 phase ($a = b = c = 10.12$ Å, $V = 1036.43/10^6$ pm^3).

Microstructure of IMO films was investigated by means of field emission scanning electron microscopy (FEG-SEM, Leo Supra 35). SEM observations were performed both on plane-view surfaces and on cross-sections of samples fractured in liquid nitrogen, in order to evaluate the coating average thickness.

Film optical transmittance (T%) was recorded by an UV–vis–NIR double beam spectrophotometer (Perkin-Elmer Lambda 19), using a bare glass substrate in the path of the reference beam in the following conditions: wavelength range 200–2800 nm, resolution 3 nm, scan rate 240 nm/min, slit 2 nm.

3. Results and discussion

3.1. Optimisation of the precursor solution

Three different routes, namely I, II and III, were followed, using different precursors and solvents.

The precursor salt concentration was also varied in the range 0.1–2.0 M in order to properly identify the optimal one. In fact, it is well known that the precursor concentration plays a strong influence on film formation, transparency and quality [32]. In all cases, on the ground of the thermal analysis results, the optimal thermal cycle parameters were selected. In Fig. 1 the TG and

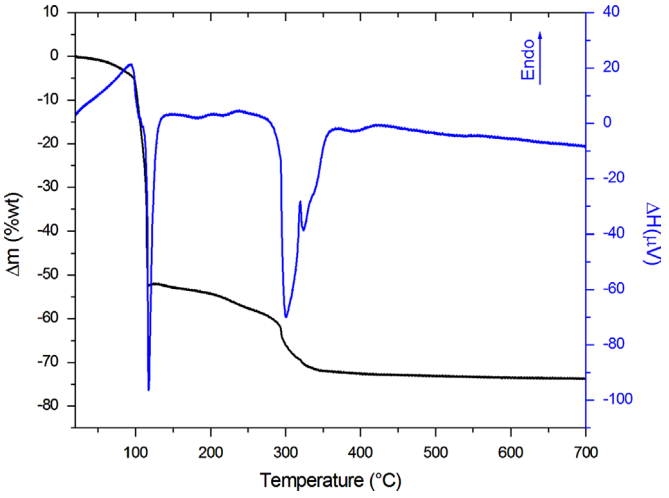

Fig. 1. TG–DTA curves of the NC3_PEG sol–gel.

DTA curves of NC3_PEG sol–gel are reported as an example, showing all samples comparable thermal behaviour. Three main weight losses were detected: the first one was ascribed to the solvent removal, the other ones to the PEG and organic components decomposition. Therefore the proper annealing temperature must be higher than 350 °C, since this is the minimum temperature necessary to remove all the contaminants, and lower than 550 °C, using glass substrates.

Route I: different solutions were prepared, using as solvent either deionised water (dH_2O) or a mixture water:ethanol (dH_2O:EtOH) 1:1, with and without the PVA addition. In the case of the aqueous solution, the presence of PVA provided an increased viscosity and an improved wetting of the glass support, allowing to obtain a coating, but opalescent and characterised by the presence of inhomogeneities (Fig. 2a), probably due to the low and difficult evaporation of water at room temperature, during the drying step.

These macroscopic evidences were confirmed by the SEM investigation (Fig. 2b–d). The coating produced in the absence of PVA (i.e. N1) revealed a smooth surface suddenly interrupted by the detrimental presence of large inhomogeneous areas, whereas the PVA addition allowed to obtain an uniform coating characterised by the presence of crystalline grains, as evident in the high magnification SEM micrograph (i.e. N1_PVA, Fig. 2d).

On the basis of these experimental evidences, the solution was prepared using as solvent a mixture of H_2O:EtOH 1:1, without the PVA (i.e. N2), obtaining a better volatility of the solvent, even if the absence of the polymer prevented the complete coating of the substrate, as evident from the comparison between the related digital pictures (Fig. 2a).

The XRD results corroborated the crystalline nature of the produced coating. In fact, the XRD pattern of the film obtained after three depositions and thermal treatment at 500 °C for 2 h was characterised by the typical diffraction peaks of the In_2O_3 (JCPDS # 76-0152) and a broad band around $2\vartheta = 22^\circ$ which testified the presence of a residual amorphous component of the coating (Fig. 3). It was not possible to detect the contribution of the below glass substrate, suggesting the deposition of a thick film. Moreover, the average crystallite size was estimated by means of the Scherrer equation, using the half width of the (222) peak, obtaining a value of 21.2 nm.

Route II: different solvents (i.e. deionized water) and mixture of solvents (i.e. methanol:glacial acetic acid (MeOH:GAA) 1:1 and ethanol:glacial acetic acid (EtOH:GAA) 1:1) were employed. The strong influence of the used solvent on the transparency of the produced coatings is macroscopically evident from the comparison between the digital pictures (insets of Fig. 4). It is clear that the aqueous solutions led to the formation of transparent films, even if not uniform (i.e. C1 and C1_PVA), whereas the employment of the mixture

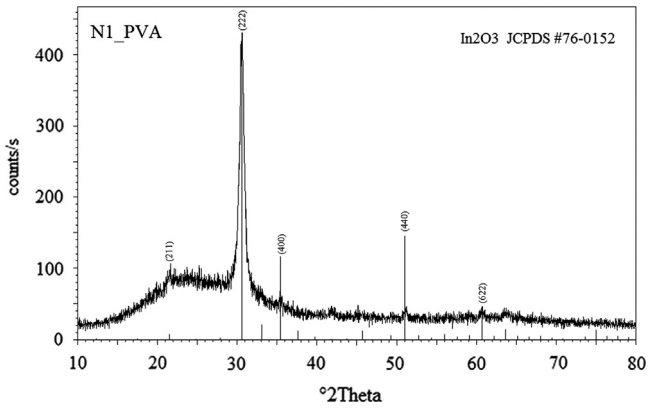

Fig. 3. Diffraction pattern of the Route I derived film after thermal treatment at 500 °C.

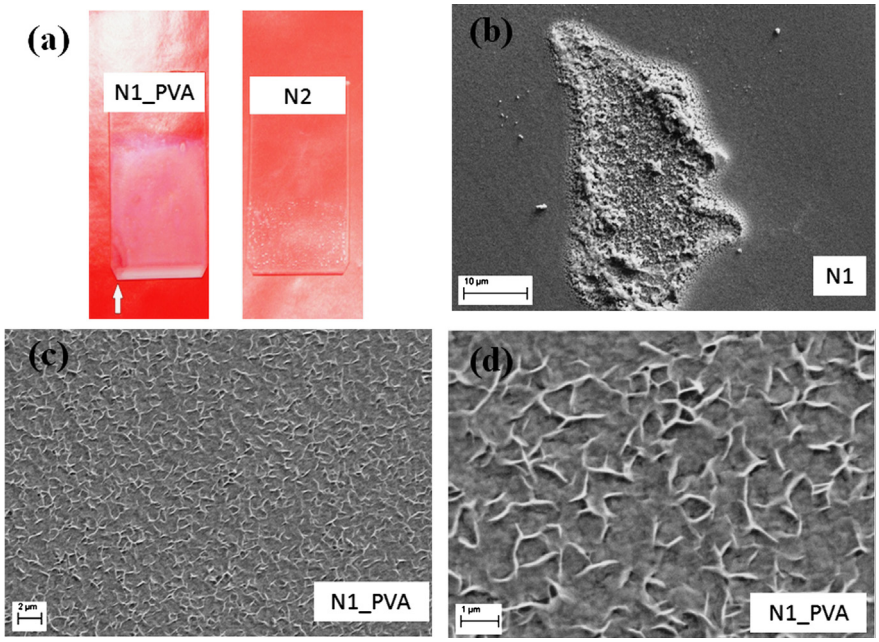

Fig. 2. (a) Photographs and (b)–(d) SEM micrographs of the Route I derived coatings (white arrow: evident defects).

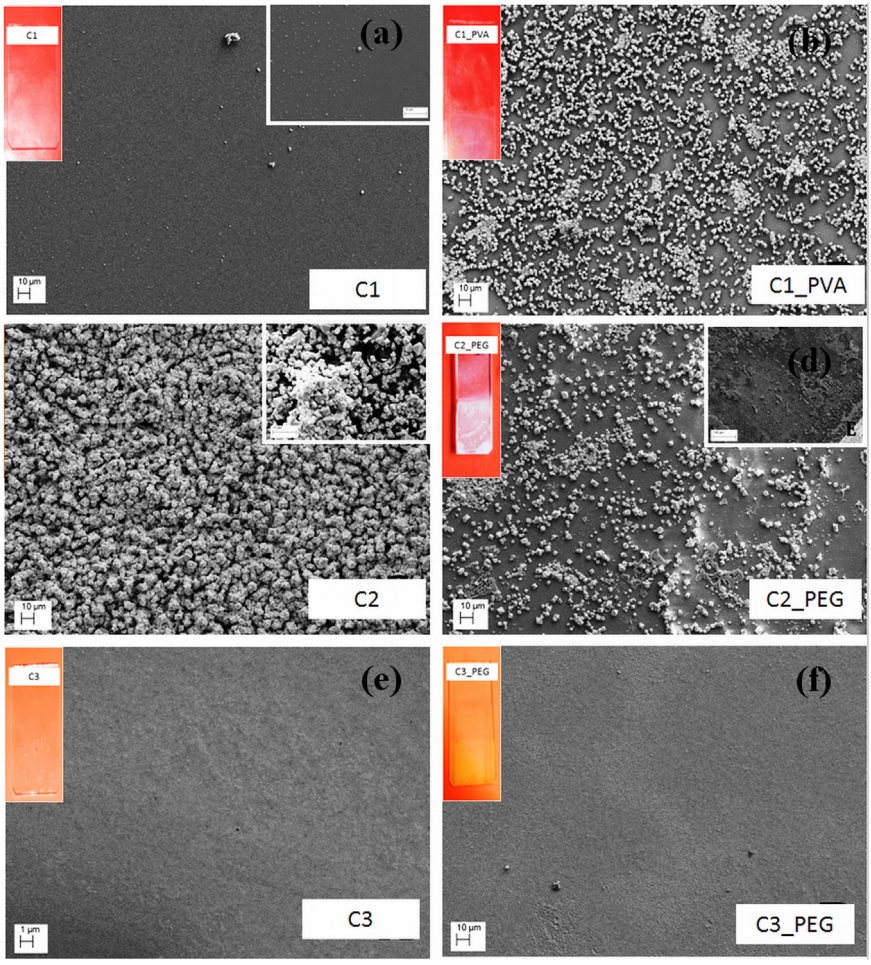

Fig. 4. SEM micrographs of the Route II derived films (inset: photographs and higher magnification images).

methanol:glacial acetic acid (1:1) resulted in opalescent coatings (i.e. C2 and C2_PEG), independently from the use of the polymeric component.

Accordingly, the SEM micrographs of the samples C1, C1_PVA, C2 and C2_PEG showed the presence of many diffuse particles, regardless of the solvent kind and of the polymeric component addition which did not seem to favour the film formation. This experimental evidence could be explained considering that when the indium chloride concentration is too high (1.0–2.0 M), the excess solute atoms may come out of the film and form the top low-adherent powdery layer that is responsible of the opalescence. The same conclusion was reported by Savarimuthu et al. in the case of the preparation of pure In_2O_3 films by the sol–gel technique [32].

It is interesting to note that the powdered layer became thicker and more crystalline increasing the solution concentration, as expected and evident from the comparison between the 1.0 M (i.e. C1) and 2.0 M (i.e. C2) samples. Remarkably reducing the starting solution concentration (i.e. 0.1–0.2 M), it was possible to observe the formation of a more uniform and fairly transparent film, as evidenced by the SEM micrographs of the films C3 and C3_PEG in Fig. 4e and f. In fact, when the indium chloride concentration decreased, most of the atoms in the film were

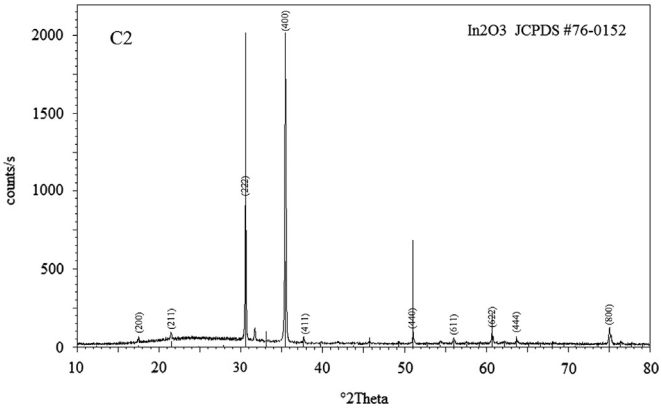

Fig. 5. XRD diffraction pattern of the thermal treated C2 film.

oxidised and well crystallised, avoiding the formation of a powdery layer [32]. Furthermore, in this case, the mixture ethanol–glacial acetic acid in a ratio 1:1 promoted the formation of transparent coatings, both with and without the PEG addition, due to the higher volatility of ethanol with respect to methanol (i.e. C3 and C3_PEG, inset of Fig. 4e and f). However, the

addition of PEG was necessary in order to obtain a uniform film which remained transparent up to six depositions.

In Fig. 5 the XRD pattern of the sample C2, after thermal treatment at 500 °C for 2 h, is reported as an example, showing the In_2O_3 (JCPDS # 76-0152) characteristic peaks. The detected peaks resulted remarkably more intense and sharper with respect to those registered for the Route I derived coatings, suggesting a high crystallinity degree, as a confirmation of the crystalline particles agglomerates observed at SEM (Fig. 4). An additional peak at $2\vartheta = 31.699^\circ$ was observed and it was ascribable neither to unwanted indium oxide nor to metallic Mo and its oxides. The presence of possible compounds whose schedules is not available in the PCPDFWIN database cannot be ruled out.

The average dimension of the crystallites was estimated and resulted, as expected, remarkably higher than those found in coatings derived from Route I (343.2 nm vs. 21.2 nm). Only for this sample, due to its higher crystallinity degree, it was possible to calculate the reticular parameters (i.e. $a=b=c=10.1199(3)$ Å, $V=1036.410/10^6$ pm^3), that resulted comparable to those reported in the JCPDS card of the cubic In_2O_3 (JCPDS # 76-0152, $a=b=c=10.12$ Å, $V=1036.43/10^6$ pm^3), demonstrating that the Mo incorporation within the In_2O_3 lattice did not alter cell structure. Moreover, it is worthy to note that Route II derived samples showed (400) as a preferential direction of growth, instead of (200).

This experimental evidence was also reported by Parthiban et al. [10,30] and Prince et al. [33], in the case of spray pyrolysed Mo-doped and undoped In_2O_3 films, respectively, using $InCl_3$ and $MoCl_5$ as In and Mo source, suggesting that, in our case, it could be imputable to the followed synthesis process, maintaining constant the thermal treatment and the Mo content.

Route III: on the ground of the experimental findings obtained with Routes I and II, the coatings were prepared starting from solutions based on indium nitrate and Mo chloride, using different solvents and concentrations, with and without polymer addition.

In details, the coatings obtained using water and PVA (i.e. NC1_PVA) presented diffuse porosities and cracks in the bottom region where the film tended to be thicker, as evidenced in the SEM micrographs shown in Fig. 6a and b.

Using the mixture ethanol:acetic acid 1:1 allowed to obtain a better deposition, obviously ascribed to the higher volatility of ethanol with respect to water, as evident from the digital picture of the sample NC2_PEG (inset of Fig. 6b).

Accordingly, the SEM investigation revealed the formation of homogeneous cracks-free films after the thermal treatment, especially in the case of samples produced from NC2_PEG and NC3_PEG precursor solutions (Fig. 6c and d).

Moreover this procedure consented to obtain transparent films up to eight depositions, as evident from the comparison between the coating NC3_PEG after six and eight steps (inset of Fig. 6d).

In Fig. 7a a comparison between the XRD diffraction patterns of the undoped In_2O_3 and Mo-doped In_2O_3 (i.e. NC2_PEG and NC3_PEG) is reported. In all cases, a unique crystalline phase (In_2O_3, JCPDS # 76-0152) was observed. It is worthy pointing out that the Mo doping induced and promoted the crystallisation of the In_2O_3 phase. In fact, more crystalline materials were obtained in the case of Mo-doped samples, increasing the intensity of the diffraction peaks with precursor concentration, as evident from the comparison between the films NC2_PEG ($[In(NO_3)_3]=0.1$ M) and NC3_PEG ($[In(NO_3)_3]=0.2$ M). In particular, the average crystallite sizes resulted 16.9, 15.8 and 23.7 nm for pure In_2O_3, NC2_PEG and NC3_PEG samples, respectively. The obtained values were comparable to the Route I-derived coatings and remarkably lower than the Route II-derived ones, as expected.

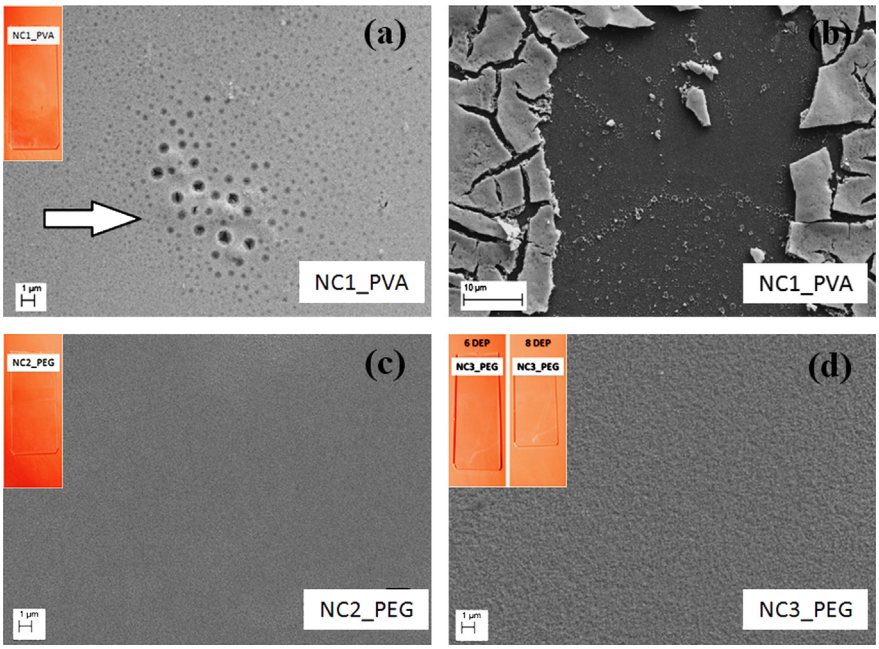

Fig. 6. SEM micrographs of the Route III derived coatings: (a) and (b) NC1_PVA, (c) NC2_PEG and (d) NC3_PEG (inset: (a)) white arrow: evident defects; (a)–(d) photographs; (d) comparison between the photographs after six and eight depositions).

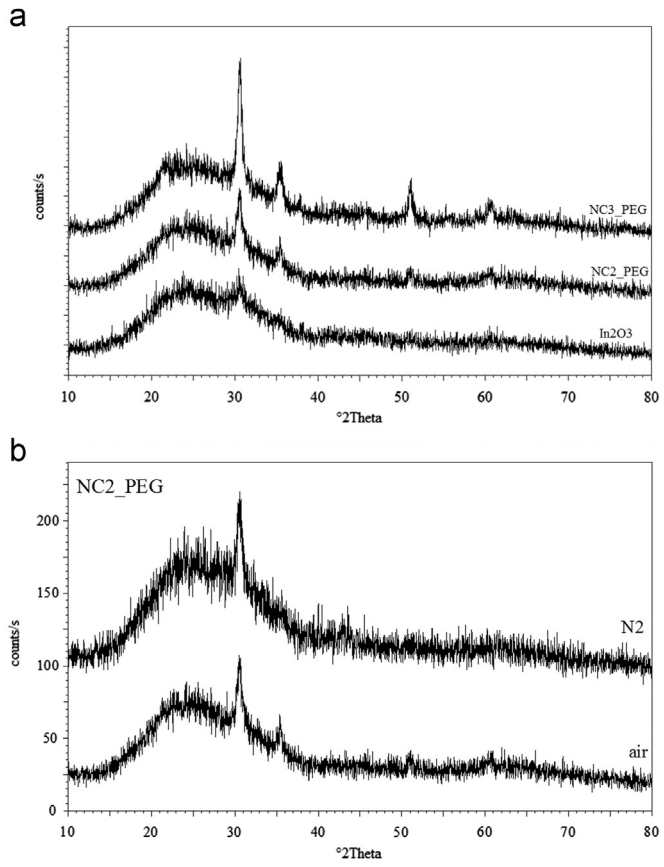

Fig. 7. XRD diffraction patterns of the coatings: (a) In_2O_3, NC2_PEG and NC3_PEG; and (b) NC2_PEG after thermal treatment in air and N_2 atmospheres.

Finally, the XRD patterns of NC2_PEG film thermally treated at 500 °C in air and in nitrogen atmospheres are very similar (Fig. 7b), implying that neither the degree of crystallinity nor the crystallites size are affected by the post-annealing atmospheres, in agreement with the literature findings [34,35].

3.2. Optical properties

Fig. 8 shows a comparison between the transmittance spectra of the IMO films produced via the three different procedures, after 6–8 dipping steps.

It is worth to remark that, due to the deposition process, both sample surfaces were coated. The Route I derived samples showed a transmittance value between 75% and 82% in the vis range, comparable to the undoped In_2O_3 film and lower than that showed by samples from Route III (i.e. 95%), accordingly with the other characterisations.

As expected, the Route II derived coatings showed transmittance values in the range 40–52%, remarkably lower than those found in Route I derived samples, in good agreement with the macroscopic evidence (insets of Fig. 4) which revealed a visible opalescent aspect.

Finally, the best optical properties were registered for coatings from Route III which showed transmittance values between 85% and 98% in the vis range.

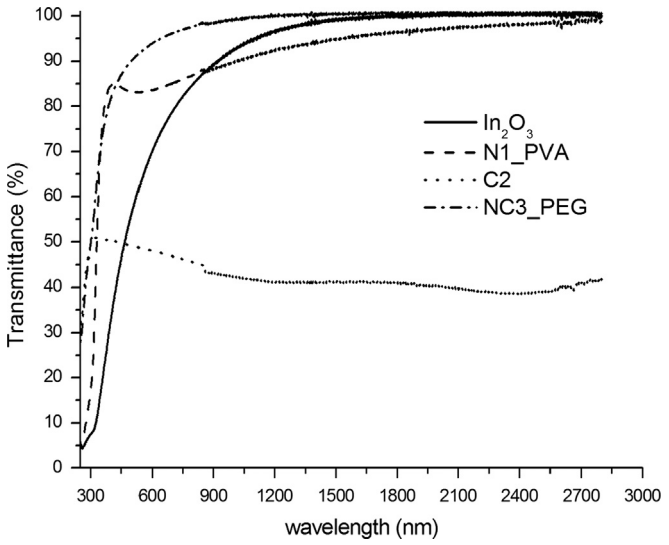

Fig. 8. Transmittance spectra of the coatings In_2O_3, N1_PVA, C2 and NC3_PEG.

The high transmittance values can be attributed to the increase of structural homogeneity and crystallinity. Indeed, the steeper optical absorption curves indicate an improved crystallinity of the films and lower defect density near the band edge, due to the annealing at high temperatures. In fact, it is well known that porosity, crystallinity, structural and surface homogeneity greatly influence film transmission [35]. A high porosity tends to increase the transmittance, while low crystallinity, poor surface and structural homogeneity to reduce it. In the case of low film thickness (low number of coatings), the dominant effect appears to be the porosity, and the transmittance could be high, in agreement with Kim et al. [35]. On the other hand, in the case of thick coatings (high number of depositions), the porosity decreases leading to reduced transmission, but the improved crystallinity and surface homogeneity cause an increment of the transmittance [36]. Under these contrasting effects, the transmittance may become more or less a constant at a certain film thickness.

4. Conclusions

Transparent molybdenum doped indium oxide coatings were successfully obtained by the dip-coating technique. The sol–gel process was properly set-up, testing different reagents (i.e. indium nitrate or indium chloride and molybdenum chloride or ammonium molybdate as In and Mo sources) and solvents. Indium nitrate and molybdenum chloride were identified as optimal In and Mo sources. The use of a mixture of ethanol:acetic acid in a 1:1 ratio as solvents, a proper concentration of In source (0.1–0.2 M) and the addition of PEG were necessary and fundamental in order to obtain uniform, homogeneous and crack-free films. The set-up procedure (dipping–drying–heating at 500 °C) was repeated several times (up to eight times), giving rise to multilayer crystalline IMO films, as confirmed by both SEM and XRD investigations. It was demonstrated that the employed annealing atmosphere (i.e. air or N_2) did not seem to play any rule and effect on the crystallinity degree and crystallites size.

This procedure allowed to obtain transparent films up to eight depositions, presenting very high transmittance values in the vis range (i.e. 85–98%).

Acknowledgements

The authors wish to acknowledge Prof. M. Casalboni and Dr. F. De Matteis, University of Rome Tor Vergata, Rome (Italy), for UV–vis facilities.

References

[1] L. Castañeda, Present status of the development and application of transparent conductors oxide thin solid films, Materials Sciences and Applications 2 (2011) 1233–1242.
[2] A.V. Moholkar, S.M. Pawar, K.Y. Rajpure, V. Ganesan, C.H. Bhosale, Effect of precursor concentration on the properties of ITO thin films, Journal of Alloys and Compounds 464 (2008) 387–392.
[3] L. Kong, J. Ma, F. Yang, C. Luan, Z. Zhu, Preparation and characterization of $Ga_{2x}In_{2(1-x)}O_3$ films deposited on ZrO_2 (100) substrates by MOCVD, Journal of Alloys and Compounds 499 (2010) 75–79.
[4] M. Sasaki, K. Yasui, S. Kohiki, H. Deguchi, S. Matsushima, M. Oku, T. Shishido, Cu doping effects on optical and magnetic properties of InO_2, Journal of Alloys and Compounds 334 (2002) 205–210.
[5] T. Asikainen, M. Ritala, M. Leskela, Atomic layer deposition growth of zirconium doped In_2O_3 films, Thin Solid Films 440 (2003) 152–154.
[6] H.K. Kim, C.C. Li, G. Nykolak, P.C. Becker, Photoluminescence and electrical properties of erbium-doped indium oxide films prepared by RF sputtering, Journal of Applied Physics 76 (1994) 8209–8211.
[7] N. Ito, Y. Sato, P.K. Song, A. Kaijio, K. Inoue, Y. Shigesato, Electrical and optical properties of amorphous indium zinc oxide films, Thin Solid Films 496 (2006) 99–103.
[8] B. Houng, C.C. Liu, M.T. Hung, Structural, electrical and optical properties of molybdenum-doped TiO_2 thin films, Ceramics International 39 (4) (2013) 3669–3676.
[9] Y. Meng, X. Yang, H. Chen, J. Shen, Y. Jiang, Z. Zhang, Z. Hua, A new transparent conductive thin film In_2O_3:Mo, Thin Solid Films 394 (2001) 218–222.
[10] S. Parthiban, K. Ramamurthi, E. Elangovan, R. Martins, E. Fortunato, R. Ganesan, High-mobility molybdenum doped indium oxide thin films prepared by spray pyrolysis technique, Materials Letters 62 (2008) 3217–3219.
[11] S.-Y. Han, G.S. Herman, C.-H. Chang, Low-temperature, high-performance, solution-processed indium oxide thin-film transistors, Journal of the American Chemical Society 133 (2011) 5166–5169.
[12] B. Sun, R.L. Peterson, H. Sirringhaus, K. Mori, Low-Temperature sintering of in-plane self-assembled ZnO nanorods for solution-processed high-performance thin film transistors, Journal of Physical Chemistry C 111 (2007) 18831–18835.
[13] D.-H. Lee, Y.-J. Chang, G.S. Herman, C.-H. Chang, A general route to printable high-mobility transparent amorphous oxide semiconductors, Advanced Materials 19 (2007) 843–847.
[14] Y.-J. Chang, D.-H. Lee, G.S. Herman, C.H. Chang, High-performance, spin-coated zinc tin oxide thin-film transistors, Electrochemical and Solid-State Letters 10 (2007) H135–H138.
[15] H.C. Cheng, C.F. Chen, C.Y. Tsay, Transparent ZnO thin film transistor fabricated by sol–gel and chemical bath deposition combination method, Applied Physics Letters 90 (2007) 012113 (3 pages).
[16] C.G. Choi, S.-J. Seo, B.-S. Bae, Solution-processed indium-zinc oxide transparent thin-film transistors, Electrochemical and Solid-State Letters 11 (2008) H7–H9.
[17] H.S. Kim, P.D. Byrne, A. Facchetti, T.J. Marks, High performance solution-processed indium oxide thin-film transistors, Journal of the American Chemical Society 130 (2008) 12580–12581.
[18] S.T. Meyers, J.T. Anderson, C.M. Hung, J. Thompson, J.F. Wager, D. A. Keszler, Aqueous inorganic inks for low-temperature fabrication of ZnO TFTs, Journal of the American Chemical Society 130 (2008) 17603–17609.
[19] C.S. Li, Y.-N. Li, Y.-L. Wu, B.-S. Ong, R.-O. Loutfy, Fabrication conditions for solution-processed high-mobility ZnO thin-film transistors, Journal of Materials Chemistry 19 (2009) 1626–1634.
[20] D.H. Lee, S.-Y. Han, G.S. Herman, C.-H. Chang, Inkjet printed high-mobility indium zinc tin oxide thin film transistors, Journal of Materials Chemistry 19 (2009) 3135–3137.
[21] M.J. Alam, D.C. Cameron, Optical and electrical properties of transparent conductive ITO thin films deposited by sol–gel process, Thin Solid Films 377–378 (2000) 455–459.
[22] S. Mohammadi, H. Abdizadeh, M.R. Golobostanfard, Opto-electronic properties of molybdenum doped indium tin oxide nanostructured thin films prepared via sol–gel spin coating, Ceramics International 39 (2013) 6953–6961.
[23] M. Kevin, G.H. Lee, G.W. Ho, Non-planar geometries of solution processable transparent conducting oxide: from film characterization to architectured electrodes, Energy and Environmental Science 5 (2012) 7196–7202.
[24] D. Uhlmann, T. Suratwala, K. Davidson, J. Boulton, G. Teowee, Sol–gel derived coatings on glass, Journal of Non-Crystalline Solids 218 (1997) 113–122.
[25] C. Terrier, J. Chatelon, R. Berjoan, J. Roger, Sb-doped SnO_2 transparent conducting oxide from the sol–gel dip-coating technique, Thin Solid Films 263 (1995) 37–41.
[26] M.G. Minett, J.R. Owen, Vanadium and titanium oxides prepared by hydrolysis of alkoxides as insertion electrodes in lithium cells with polymeric electrolytes, Journal of Power Sources 32 (1990) 81–97.
[27] A.E. Gash, J.H. Satcher Jr., R.L. Simpson, Strong akaganeite aerogel monoliths using epoxides: synthesis and characterization, Chemistry of Materials 15 (2003) 3268–3275.
[28] A.E. Gash, T.M. Tillotson, J.H. Satcher Jr., L.W. Hrubesh, R.L. Simpson, New sol–gel synthetic route to transition and main-group metal oxide aerogels using inorganic salt precursors, Journal of Non-Crystalline Solids 285 (2001) 22–28.
[29] A.E. Gash, T.M. Tillotson, J.H. Satcher Jr., J. Poco, L.W. Hrubesh, R.L. Simpson, Use of epoxides in the sol–gel synthesis of porous iron(III) oxide monoliths from Fe(III) salts, Chemistry of Materials 13 (2001) 999–1007.
[30] S. Parthiban, V. Gokulakrishnan, K. Ramamurthi, E. Elangovan, R. Martins, E. Fortunato, R. Ganesan, High near-infrared transparent molybdenum-doped indium oxide thin films for nanocrystalline silicon solar cell applications, Solar Energy Materials and Solar Cells 93 (2009) 92–97.
[31] S. Parthiban, K. Ramamurthi, E. Elangovan, R. Martins, E. Fortunato, Spray deposited molybdenum doped indium oxide thin films with high near infrared transparency and carrier mobility, Applied Physics Letters 94 (2009) 212101 (3 pages).
[32] E. Savarimuthu, K.C. Lalithambika, A.Moses Ezhil Raj, L.C. Nehru, S. Ramamurthy, A. Thayumanavan, C. Sanjeeviraja, M. Jayachandran, Synthesis and materials properties of transparent conducting In_2O_3 films prepared by sol–gel-spin coating technique, Journal of Physics and Chemistry of Solids 68 (2007) 1380–1389.
[33] J.J. Prince, S. Ramamurthy, B. Subramanian, C. Sanjeeviraja, M. Jayachandran, Spray pyrolysis growth and material properties of In_2O_3 films, Journal of Crystal Growth 240 (2002) 142–151.
[34] Y. Djaoued, V.H. Phong, S. Badilescu, P.V. Ashrit, F.E. Girouard, V.V. Truong, Sol–gel-prepared ITO films for electrochromic systems, Thin Solid Films 293 (1997) 108–112.
[35] S.-S. Kim, S.-Y. Choi, C.-G. Park, H.-W. Jin, Transparent conductive ITO thin films through the sol–gel process using metal salts, Thin Solid Films 347 (1999) 155–160.
[36] J. Liu, D. Wu, S. Zeng, Influence of temperature and layers on the characterization of ITO films, Journal of Materials Processing Technology 209 (2009) 3943–3948.